3D Electron Diffraction: The Nanocrystallography Revolution

Mauro Gemmi,*,† Enrico Mugnaioli,† Tatiana E. Gorelik,‡ Ute Kolb,§,∥ Lukas Palatinus,⊥ Philippe Boullay,# Sven Hovmöller,∇ and Jan Pieter Abrahams○,◆,¶

†Center for Nanotechnology Innovation@NEST, Istituto Italiano di Tecnologia, Piazza S. Silvestro 12, 56127 Pisa, Italy

‡University of Ulm, Central Facility for Electron Microscopy, Electron Microscopy Group of Materials Science (EMMS), Albert Einstein Allee 11, 89081 Ulm, Germany

§Institut für Anorganische Chemie und Analytische Chemie, Johannes Gutenberg-Universität, Duesbergweg 10-14, 55128 Mainz, Germany

∥Institut für Angewandte Geowissenschaften, Technische Universität Darmstadt, Schnittspahnstraße 9, 64287 Darmstadt, Germany

⊥Department of Structure Analysis, Institute of Physics of the CAS, Na Slovance 2, 182 21 Prague 8, Czechia

#CRISMAT, Normandie Université, ENSICAEN, UNICAEN, CNRS UMR 6508, 6 Bd Maréchal Juin, F-14050 Cedex Caen, France

∇Inorganic and Structural Chemistry, Department of Materials and Environmental Chemistry, Stockholm University, 106 91 Stockholm, Sweden

○Center for Cellular Imaging and NanoAnalytics (C−CINA), Biozentrum, Basel University, Mattenstrasse 26, CH-4058 Basel, Switzerland

◆Department of Biology and Chemistry, Paul Scherrer Institut (PSI), CH-5232 Villigen PSI, Switzerland

¶Leiden Institute of Biology, Leiden University, Sylviusweg 72, 2333 BE Leiden, The Netherlands

ABSTRACT: Crystallography of nanocrystalline materials has witnessed a true revolution in the past 10 years, thanks to the introduction of protocols for 3D acquisition and analysis of electron diffraction data. This method provides single-crystal data of structure solution and refinement quality, allowing the atomic structure determination of those materials that remained hitherto unknown because of their limited crystallinity. Several experimental protocols exist, which share the common idea of sampling a sequence of diffraction patterns while the crystal is tilted around a noncrystallographic axis, namely, the goniometer axis of the transmission electron microscope sample stage. This Outlook reviews most important 3D electron diffraction applications for different kinds of samples and problematics, related with both materials and life sciences. Structure refinement including dynamical scattering is also briefly discussed.

1. INTRODUCTION

Accelerated electrons have been long considered the less promising among the radiation types used in crystallography for attaining diffraction data suitable for atomic structure determination. In fact, the large majority of structural models deposited in crystallographic databases[1−5] have been obtained by means of X-ray diffraction, and most of what is left has been derived from neutron diffraction or spectroscopic methods. Although still limited, the use of electron diffraction has grown rapidly over the past decade, mostly due to the introduction of 3D methods for the systematic acquisition and analysis of diffracted intensities. Here, we would like to examine how the use of parallel beam electron diffraction for structure determination has evolved from a mostly qualitative technique, used only by few specialists, to a quantitative approach accessible to a much larger community.

To understand the full picture of this (r)evolution, it is important to focus on the strengths of accelerated electrons for

crystallography. First, the possibility to have parallel electron probes with a size of a few nanometers allows collecting diffraction data from sample volumes 2 or 3 orders of magnitude smaller than the ones suitable for synchrotron microfocused X-ray beams. Second, the ability to deliver both diffraction and imaging from the same nanovolume allows the combination of reciprocal and direct space information and the experimental determination of crystallographic phases. Third, the strong Coulomb interaction between electrons and matter allows a good signal-to-noise ratio even from very thin samples and an easier identification of light atoms, like lithium and hydrogen, when compared with X-rays.

However, the strong scattering of electrons is also the reason why electron diffraction (ED) was disregarded for many years for structure analysis. The occurrence of multiple scattering

events (dynamical effects) while electrons pass through the sample has a significant impact on the intensities of Bragg reflections.[6,7] In diffraction data, the structure information dwells in the relative differences between reflection intensities, and it is evidently lost or jeopardized when such intensities are leveled out, or their ranking is scrabbled due to multiple scattering.

ED experienced a true rebirth in the past 20 years of the past century, thanks to the research of Dorset and co-workers[8,9] and Hovmöller and co-workers,[10,11] that demonstrated how ED data acquired in a transmission electron microscope (TEM) can be used for the structure characterization of both organic and inorganic nanocrystalline samples, despite the presence of dynamical effects. Shortly after, Gonen et al.[12] also showed that ED can be used for the structure determination of 2D protein crystals at almost-atomic resolution. Still, the occurrence of multiple scattering[13] and the difficulty in merging intensities between different ED patterns[14] hindered the application of classical crystallographic routines for structure determination and restricted ED to a very time-consuming and niche technique, whose fallouts often needed a further validation.

Only in 2007 researchers started to realize that limitations of ED were mostly related with the data collection strategy. Thus far, ED data were always acquired after orienting a target crystal along low-index and well recognizable crystallographic axes. This procedure evidently cuts down the number of recorded reflections. Additionally, in low-index in-zone patterns dynamical effects are just maximized by the simultaneous excitation of many, geometrically related reflections.

As an alternative, Kolb and co-workers[15-18] proposed acquiring ED patterns *off-zone*, after tilting the sample in fixed angular steps around an arbitrary, noncrystallographic axis. In fact, this procedure just mimics data acquisition by a simple monoaxial diffractometer equipped with an area detector. Each single diffraction pattern cannot be easily interpreted alone, but once the angular relationship between the patterns is known, the whole data set can be reconstructed into a 3D volume from which cell parameters, extinction rules, and reflection intensities are conveniently extracted by dedicated software.

Since 2007, the three-dimensional ED method has spread with an exponential trend. Very soon, still in the hand of few specialists, it allowed the structure determination of landmark samples, mostly inorganic, that were considered impracticable for X-ray methods.[19-28] Later, the introduction of ultrafast data acquisition procedures and of more sensitive detectors allowed establishing robust experimental protocols also for organic and metalorganic materials.[29-35] Finally, three-dimensional ED found successful applications for macromolecules[36-45] and other structures of biologic interest.[46-50] The growing attention on three-dimensional ED is confirmed by the number and impact of related publications in the very last year,[51-77] and by the fact that this method has been considered one of the most important recent scientific breakthroughs.[78]
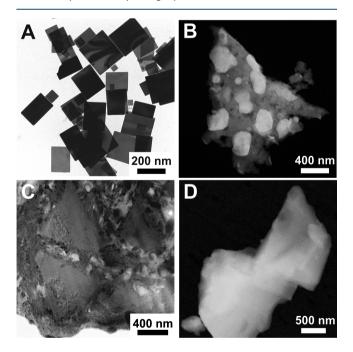
The fast spread-out of the technique without the availability of dedicated instrumentations has brought researchers to develop different experimental set-ups for data acquisition (as will be described in detail in the next section). Consequently, several acronyms are found in the literature, like automated diffraction tomography (ADT),[16] electron diffraction tomography (EDT),[79] single-crystal electron diffraction (SCED),[53] precession-assisted electron diffraction tomography (PEDT),[80] rotation electron diffraction (RED),[81,82] continuous rotation electron diffraction (cRED),[68] and microcrystal electron

diffraction (MicroED).[32,38] Nonetheless, we argue that all these variants share the same core concept, i.e., the idea of sampling the whole available three-dimensional reciprocal space by a tilt of the sample around an arbitrary axis. In this Outlook we will therefore use the generic term 3D ED when broadly referring to all of them.

Compared to conventional in-zone ED patterns, the most obvious advantage of 3D ED is that all reflections reachable in the tilt range of the TEM goniometer are sampled, thus maximizing data completeness. All at once, dynamical effects are drastically reduced, because less geometrically related reflections are excited at the same time. In fact, *ab initio* structure determination by 3D ED data is normally achieved with the same routines developed for X-ray crystallography[83-85] and without any special treatment for multiple scattering. Finally, data acquisition is significantly faster, easier, and more reproducible, allowing sampling many crystals in a short time and working on very beam sensitive materials.

3D ED is conceptually comparable to single-crystal X-ray but allows data collection from much smaller volumes. Typical crystals for 3D ED range from 10^0 to 10^{-4} μm^3. Even if XFEL radiation allows diffraction data from comparable crystals, the accessibility of dedicated facilities is still rather limited for general users.[86] Moreover, ED can easily access single crystals even in polyphasic mixtures or embedded in a solid matrix (Figure 1).

X-ray powder diffraction (XRPD) is an option for dealing with crystals with a size of few hundreds or few tens of nanometers. This method has also developed into a reliable structure analysis technique in the past decades and is remarkably accurate for what concerns cell and structure refinement. However, XRPD is intrinsically limited by the projection of the information onto

Figure 1. Examples of crystals suitable for 3D ED data collection. (A) $Cu_{2-x}Te$ nanoplatelets, with lateral size of 100−200 nm and thickness of few tens of nanometers. (B) Submicrometric $Eu_2Si_2O_7$ grains embedded in a ground mass of nanocrystalline quartz. (C) Submicrometric cronstedtite pyramidal crystals in a focused ion beam (FIB) lamella, sampled from the carbonaceous meteorite Paris. (D) Micrometric pharmaceutical crystal.

one dimension. Systematic and accidental peak overlap is a well-known issue when dealing with structures with long cell parameters or pseudosymmetries. A small crystal size and occurrence of defects result in peak broadening and asymmetry, which in turn emphasize overlapping. Moreover, when the sample of interest is a polyphasic mixture, the XRPD signal is the superposition of reflections from all crystalline components, further hampering any structural interpretation.

In the past years, the potential of electrons for crystallography has become evident due to the outburst of cryo-EM imaging for macromolecule single-particle determination.[87,88] Similarly, 3D ED requires relatively small crystals and can be applied to crystallization products that are considered failures in the eyes of X-ray crystallographers.[31,32] Additionally, ED allows for a better structural resolution and requires an electron dose much lower than any imaging technique, as testified by the successful structure determinations of very beam sensitive materials,[21,26,30,35,46−50,56,68,73] possibly even without the need of cooling down the sample.[24,29,34,55,62]

> 3D ED requires relatively small crystals and can be applied to crystallization products that are considered failures in the eyes of X-ray crystallographers

2. DATA COLLECTION PROTOCOLS

A 3D ED data set is essentially a sequence of diffraction patterns recorded sequentially at different tilt angles of the TEM goniometer. The tilt axis is the goniometer axis of the TEM stage, and its angular range is limited by the presence of the objective lens pole pieces, so that in a standard setup the tilt range cannot exceed 120° (±60°). Thus, differently from singly-crystal X-ray diffraction, there is an intrinsic limitation to the reciprocal space coverage due to the fact the TEM is primarily built to perform as a microscope and not as a diffractometer.

The simplest data collection strategy consists in a stepwise tilt of the crystal in fixed angular steps, with the acquisition of an ED pattern at each tilt stage (Figure 2A).[15] The reciprocal space reconstructed from the collected patterns allows for a reliable unit cell determination.[16] However, the recorded diffraction intensities suffer from an imprecise integration due to the gap between two sequential positions.[89] This missing wedge can be physically filled by collecting the patterns in precession mode (Figure 2B). In precession electron diffraction, the beam is tilted away from the optical axis and precessed at high speed on a conical surface with the vertex fixed on the sample plane.[90] The beam movement makes the Ewald sphere sweep the reciprocal space around the plane normal to the optical axis. This data collection procedure is often referred to as precession-assisted electron diffraction tomography (PEDT), and it has been the first 3D ED method with a high degree of success for structure determination.[17,18]

An alternative stepwise approach is the so-called rotation electron diffraction (RED), where the missing wedge is filled by fine beam tilt steps achieved using the TEM deflection coils (Figure 2C).[81,82] The angular step is this way reduced to less than 0.1°. A complete RED data collection is implemented by consecutive large mechanical tilts (2−3°), followed every time by a sequence of patterns collected in fine electrical beam tilts.
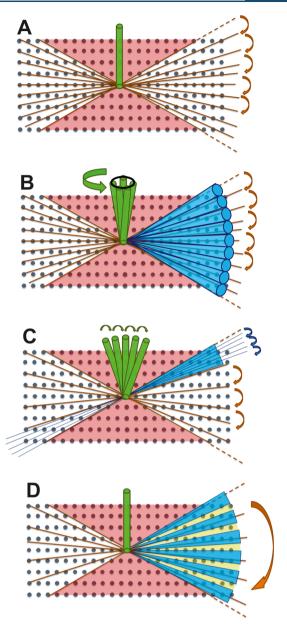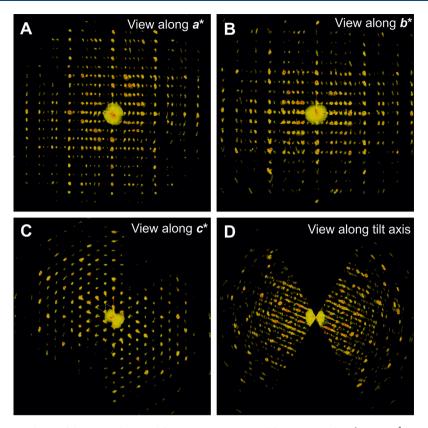

Figure 2. Sketches of the four main 3D ED data collection protocols. (A) Simple stepwise acquisition performed with fixed mechanical tilt steps (brown arrows) and steady beam (in green). The tilt step is normally 0.5−2°. (B) Stepwise acquisition performed with fixed mechanical tilt steps (brown arrows) while the beam is precessing around a conical surface pointed on the sample (green arrow). The Ewald sphere is also precessing (blue cones), and this movement allows a better integration of the Bragg reflection intensities. (C) Stepwise RED acquisition. Large mechanical tilt steps (brown arrows) are followed by small beam tilt steps (green arrows) obtained by the deflection coils of the TEM. The beam tilt step may be smaller than 0.1°. (D) Continuous rotation acquisition. The sample is mechanically tilted within the whole goniometer range (brown arrow) while the detector is acquiring a sequence of patterns. The acquisition tilt step is determined by the sum of exposure time (blue) and readout time (yellow). The latter is also responsible for the nonsampled wedges between two consecutive patterns. The beam is stationary during the whole data acquisition, and the main limit is given by the goniometer stability, because the sample tends to shift laterally during the tilt and therefore may go out from the illuminated area. The not sampled missing wedge is exaggerated in the figures and is colored in red. It is the same for all acquisition protocols, as it depends only on the mechanical limit of the TEM goniometer.

Figure 3. Exemplary diffraction volume of the trigonal mineral franzinite reconstructed from 3D ED data (a = 12.9 Å, c = 26.6 Å). (A) View along a^*. (B) View along b^*. (C) View along c^*. (D) View along the tilt axis of the acquisition. Note that these are projections of a 3D volume and not conventional 2D oriented ED patterns. Cell edges are sketched in yellow. a^* vector is in red, b^* vector in green, and c^* vector in blue. Data resolution is about 0.8 Å. The figure is made by ADT3D software.[18]

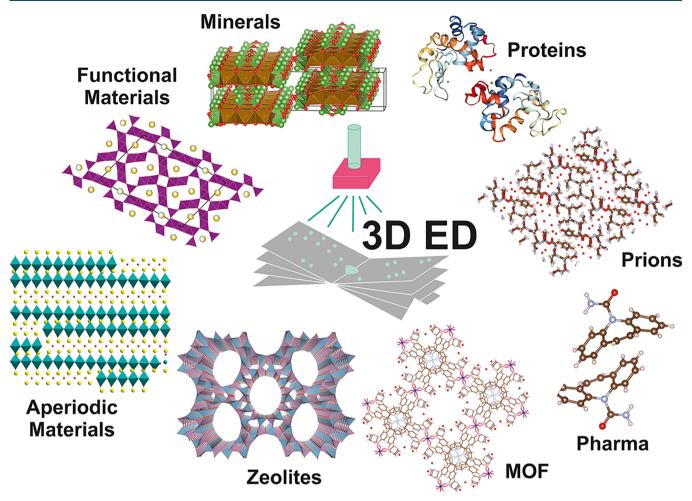The total number of patterns is on the order of 1000, about 10 times more than in PEDT.

The crystals analyzed in 3D ED are usually smaller than 1 μm; therefore, any mechanical instability of the goniometer can easily bring the crystal out of the illuminated area. In both RED and PEDT, after each mechanical tilt step the crystal position is checked by recording a TEM or STEM image, and if necessary, unwanted sample shifts are corrected by recentering the crystal under the beam. The first 3D ED data collection protocol that appeared in the literature, generally referred as automated diffraction tomography (ADT), is entirely working in STEM mode with a nanosized and adjustable quasiparallel beam. An automatic crystal tracking by STEM imaging allows compensating the mechanical drift through an equivalent shift of the electron beam.[15,91]

The third and most recent approach to 3D ED is based on a continuous data collection while the goniometer is rotating (Figure 2D).[36] In this case the missing wedge is directly sampled by the detector, which is recording the diffracted intensities during the rotation, as it is done in oscillation singly-crystal X-ray diffraction. Differently from X-rays, the rotation never stops during data collection to minimize any mechanical instability. Thus, the relation between the detector exposure and the goniometer rotation speed determines the effective angular step. The continuous data collection relies on the high stability of the goniometer, since crystal recentering is impossible, and on the speed of the detector, which should be fast enough to avoid loss of reciprocal space sampling during readout time. Data collection in continuous rotation is known under different names, as MicroED,[38] IEDT,[89] or cRED.[30] This data collection

strategy is the one that guarantees the minimum electron dose on the sample and currently is the one most commonly used for structure determination of beam sensitive materials like small organic molecules,[29−32] proteins,[38−44] and protein fragments.[46−50]

Regardless of the chosen data collection protocol (PEDT, RED, or continuous rotation) the crystal can be illuminated either in selected area mode (SAED) or in parallel nano-diffraction mode (NED). In SAED mode the target area is selected by an SAED diaphragm located in the postsample image plane, and therefore, the illuminated portion of the sample is larger than the area used for collecting diffraction data. If the sample is beam sensitive, the beam damages the whole crystal and not only the area visible inside the SAED aperture. On the contrary, in NED mode the diffracting area is selected by inserting a small presample condenser aperture. The sample is illuminated with a parallel beam having a size in the 50−200 nm range, thus avoiding damaging the part of the crystal which is not diffracting. NED gives full control on the beam diameter used and in principle also allows collecting data on a smaller area with respect to SAED. Consequently it is the method of choice in the case of low crystallinity, high mosaicity, or order−disorder polytypism at the nanoscale.[20,45,58,61,92−95]

PEDT and RED, allowing crystal tracking and recentering in image mode, guarantee that the crystal is always perfectly illuminated up to the tilt limit of the TEM goniometer and therefore always allow the maximum reciprocal space coverage. However, in both cases the crystal is illuminated longer than is strictly required for the diffraction data collection, with an obvious increase of the total electron dose. The continuous

Figure 4. Sketch showing some representative structures solved by 3D ED method for different classes of materials. Starting from the upper left and going anticlockwise: the mineral karibibite,[133] a tunnel (Na,Mn)-oxide for electrolytic applications,[124] the aperiodic structure of $SrBi_7NbO_{24}$,[122] the extra-large-pore silicoaluminophosphate ITQ-51,[25] the cobat tetraphosphonate MOF Co-CAU-36,[66] the pharma compound carbamazepine-III,[29] the amyloid core of the Sup35 prion protein,[47] and a new monoclinic polymorph of lysozyme.[45]

rotation method, instead, assures at the same time the maximum speed and the minimum electron dose on the sample. Its implementation has been boosted by the development of radiation hard hybrid detectors that are sensible to single-electron arrivals and are very fast, with negligible readout times.[33,36,96] Exploiting the speed and the sensitivity of such detectors, it is possible to collect a full ED data set in few tens of seconds, with electron doses on the order of 0.01 el s^{-1} Å^{-2} and without any reasonable loss of reciprocal space information. However, continuous rotation does not allow crystal tracking and recentering, and therefore the crystal of interest may move out from the illuminated area, especially at high tilt. This may be a serious issue if other crystals or phases are present in the surroundings.

In the case of slow detectors with a long readout time that would be incompatible with a fast continuous data collection, data can be collected in PEDT mode by blanking the beam during the rotation and avoiding any recentering, provided the goniometer is stable. In this way the total dose coincides with the dose of a continuous rotation, and the missing gaps are sampled by precession.[97]

Usually, very sensitive samples are studied in low-temperature conditions.[21,30] However, the high sensitivity of the new hybrid detectors combined with fast rotation or STEM imaging for

crystal searching may allow data collection at room temperature before critical sample deterioration.[24,29,55,62]

The speed in data collection introduced by continuous rotation protocols makes 3D ED usable also as an overall sample checking routine for nanocrystalline polyphasic mixtures or assembles. Surveys of continuous data collection have been used for the identification of known and unknown phases[32,92,98] and may foresee possible applications of 3D ED as a quality control technique for chemical synthesis.

All the described 3D ED protocols have in common a proper integration of the reflections over the reciprocal space and a minimization of the dynamical scattering, because reflections are generally collected far from low-index zone axis orientations. Nowadays, several software suites exist for 3D ED data reduction, which allow the accurate refinement of experimental parameters, the reconstruction of the 3D diffraction volume, the 3D visualization of the data set, the determination of cell parameters, and the integration of reflection intensities (Figure 3): ADT3D,[18] EDT-PROCESS,[79] PETS,[73] and RED.[82] Moreover, software developed for X-ray crystallography can be also adapted for the analysis of ED data, like DIALS,[99] MOSFLM,[100] and XDS.[41] 3D ED intensity data can be subsequently used as kinematical "X-ray-like" input for *ab initio* structure solution via direct methods, charge flipping, simulated annealing, or

molecular replacement in almost all possible kinds of crystalline compounds, both organic and inorganic (Figure 4).

> 3D ED intensity data can be subsequently used as kinematical "X-ray-like" input for *ab initio* structure solution via direct methods, charge flipping, simulated annealing, or molecular replacement in almost all possible kinds of crystalline compounds, both organic and inorganic

3. DYNAMICAL REFINEMENT

Even if dynamical scattering is significantly reduced in 3D ED data, still a pure kinematical approximation during refinement normally results in high figures of merit, when compared to typical values for X-ray diffraction. Also, the refined structure models are generally less accurate, and there is a limited sensitivity to subtle structural features, like displacement parameters, partial atomic occupancies, and coordinates of light atoms like hydrogen.

An alternative refinement procedure was developed by Palatinus et al.[101,102] In this procedure the model intensities for the least-squares refinement are calculated using the dynamical diffraction theory.[103,104] The calculation of the intensities uses the Bloch-wave formalism, which is well-suited for the intensity calculation in general, off-zone crystal orientations. The input to the refinement procedure is diffracted intensities from a 3D ED data set obtained with beam precession.[17,90] The intensities are extracted frame by frame and are treated separately for each frame. Only reflections sufficiently integrated by the precession are used in the refinement. In addition to structural parameters, the thickness of the crystal is also refined. Attempts to use data collected without beam precession have so far failed.

The dynamical refinement improves the accuracy of the structure parameters typically by a factor of 2−3 when compared to the kinematical refinement. The average error of atomic positions is reduced to about 0.02 Å.[102] Dynamical refinement also allows a more accurate determination of atomic partial occupancies[102,105] and the location of hydrogen atoms in organic, organometallic, and even inorganic materials (Figure 5A).[56,95,105] Thanks to this enhanced sensitivity, the dynamical refinement also allows for the discrimination of atomic species with close scattering powers, like in the alloy Ni_8Ti_5,[106] and for the investigation of positional and occupational disorder in layered materials.[107]

An important feature of dynamical refinement is its strong sensitivity to the absolute configuration of noncentrosymmetric crystal structures. The correct absolute structure can be determined unambiguously not only in inorganic materials with heavy scatterers[102,108] but also in organic materials and pharmaceuticals.[73]

The calculations involving dynamical diffraction theory are much more computationally demanding than the ones necessary with a kinematical approximation. Therefore, the computing time needed for the dynamical refinement is longer than the time for the kinematical refinement and may reach several hours per refinement cycle for large structures. The computing time becomes prohibitively large for macromolecular structures, and therefore no dynamical refinement of a macromolecular crystal structure has been performed so far.

4. APPLICATIONS IN MATERIALS SCIENCES

The main strength of ED is evidently the ability of performing single-crystal diffraction on areas of few hundreds or few tens of nanometers. The probe size is eventually limited by the convergence and the coherence of the beam, which may introduce distortions in the recorded patterns. Thus far, the smallest beam size reported for 3D ED is about 30−50 nm when working in NED mode with a small condenser aperture.[15,18]

3D ED is therefore the technique of choice for the analysis of nanocrystalline mixtures, where XRPD interpretation is hampered by the overlapping signals from multiple different phases. 3D ED allows a first screening of the sample through the analysis of several single crystal grains, with a time frame of a few minutes per sampled spot.[92,98] Even faster automated systems, able to perform multiple data acquisitions from different areas of the sample, have been recently proposed.[53,109] Cell parameters can be coupled with chemical information obtained by electron-dispersive X-ray spectroscopy (EDX or EDS), allowing unequivocal recognition of all the phases already reported in crystallographic databases. Additionally, if unknown or unrecognized phases are identified, a more accurate analysis of 3D ED data should provide *ab initio* their structure determination. Remarkably, such an analytical protocol can be performed on extremely small sample batches, which cannot be conveniently prepared for XFEL, or even for conventional XRPD. Moreover, 3D ED screening does not destroy the sample, thus allowing future further investigations on the same batch or even on exactly the already analyzed crystal grains.

It is worth mentioning that structural complexity does not appear to be a real limit, at least for inorganic materials. For example, the intermetallic quasicrystal approximant $Al_{77}Rh_{15}Ru_8$[110] and the mineral charoite[20] were solved despite their asymmetric units containing 78 and 90 atoms, respectively. Also, electrons are more sensitive to light atoms, and therefore, they are able to locate more easily species like lithium[18,111] and possibly hydrogen.[56,95,105]

> electrons are more sensitive to light atoms, and therefore, they are able to locate more easily species like lithium and possibly hydrogen

3D ED is rather efficient also for the characterization of materials with pervasive disorder. The small probe size allows spotting locally ordered sample areas[92−94] and single crystal individua in twinned samples.[60,112] This ability is particularly crucial for materials where different order−disorder sequences may arise due to modifications in structural packing.[20,61,95] Additionally, recent studies quantitatively correlated 3D diffuse scattering features with structural disorder.[58,113−115]

4.1. Functional Materials. Thanks to the high sampling resolution, 3D ED allows collecting structural data from single nanoparticles, nanowires, or nanodevices. Birkel et al.[19] in one of the first pioneering papers determined the structure of a new

$Zn_{1+x}Sb$ phase obtained as 50 nm particles in a yield containing also ZnSb impurities. More recently, Willhammar et al.[116] and Mugnaioli et al.[60] analyzed the structure modulations in plasmonic $Cu_{2-x}Te$ particles combining 3D ED and high-resolution TEM and STEM imaging. Baraldi et al.[117] performed the structure determination of a new $Eu_2Si_2O_7$ phase recovered as nanoprecipitates inside a quartz matrix. Mayence et al.[118] also proposed the application of 3D ED for the study of twinned metallic particle seeds.

3D ED is an extremely promising technique for the structure determination of functional layered oxides, even if characterized by disorder[119,120] or incommensurate modulations.[64,80,121,122] 3D ED was also used for the analysis of structure modifications caused by the thermal annealing of Ni/Au electrodes,[123] and for the study of materials engineered for electrochemical applications.[59,111,124] In this regard, Karakulina et al.[57] performed the first *in situ* charge/discharge experiment on a $(Li)FePO_4$ electrode.

Another application for 3D ED resides in the structure analysis of epitaxial thin films. In addition to their intrinsically small diffracting volume, these films are clamped onto a thick crystalline substrate that significantly complicates their analysis by X-ray diffraction and limits the number of measurable reflections. 3D ED was recently used for the characterization of the multiferroic compound $Bi_3(Mn,Fe)_4O_{11}$[28] and the antiferromagnetic compound CuMnAs.[65] Additionally, 3D ED allows a straight comparison between the structure of the known bulk material and the one observed in thin films.[125] A very promising application of dynamical refinements is foreseen for such cases where the main goal is to point out subtle structural changes. Steciuk et al.[76] showed that the structure of a thin film of $CaTiO_3$ grown on $SrTiO_3$ can be refined even in the presence of twinning and that the evolution of the thin film structure as a function of the distance from the substrate may also be observed.

The 3D ED ability of analyzing single components in a nanocrystalline mixture was also applied for the study of HP syntheses[126,127] and metallic alloys.[51] 3D ED is also a powerful instrument for the characterization of intermediate synthetic snapshots, to follow a specific reaction pathway.[128,129]

4.2. Minerals. Several mineral species can be found only in the form of nanocrystals inside complex polyphasic parageneses. Moreover, many of them show polytypism, disorder, and twinning at a very fine scale, possibly associated with pseudosymmetry and severe peak overlap in XRPD. For such samples, 3D ED looks like the only technique able to deliver comprehensive structural information. This technique has already allowed the structure determination of several minerals that have been recognized for decades but whose structures were still lacking because no crystal suitable for single-crystal X-ray diffraction actually exists.[74,75,130–133] Charoite[20] and denisovite[94] embody two emblematic cases which highlight the strengths of the 3D ED method. These extremely complex minerals appear only as submicrometric fibers, typically made of different polytypic sequences stacked one next to the other in areas of few unit cell repetitions.

3D ED is also a valid option for the study of alteration products,[134] biomineralizations,[135] metamict minerals,[136] and first nucleating crystalline seeds. In this regard, it allowed the structure characterization of several hydrated and dehydrated $CaCO_3$ cryptocrystalline polymorphs.[61,77,137] Dynamical refinement also allowed a reliable refinement of Mg/Fe partial occupancies in orthopyroxene.[102] Additionally, meteorites[138] and rocks formed at nonequilibrated and extreme conditions,

like seismogenic mirror faults and shock-metamorphic impactites, typically host polyphasic grains and cryptocrystalline matrices and therefore constitute ideal candidates for the 3D ED method.[139]

3D ED is also an excellent option for the study of recovered samples from experimental mineralogy and petrology, typically consisting of small yields and nanocrystalline polyphasic assemblies.[72,92,140–142] Finally, a recent study showed interesting applications of 3D ED for the characterization of archeological finds.[69]

4.3. Porous Materials. Zeolites and other inorganic molecular sieves are optimal targets for the 3D ED method. They usually consist of rather complex 3D frameworks, associated with long cell parameters that produce XRPD peak overlap already at medium resolution. Additionally, they are typically electron beam sensitive and difficult to study by means of high-resolution TEM imaging. New frameworks are continuously engineered to tune chemical and physical properties, which are mostly structure-dependent. Still, it is not always possible to grow single crystals for X-ray diffraction, and therefore, 3D ED has quickly become one of the reference techniques for the structure determination of molecular sieves,[22,25,27,63,70,143–146] also in the presence of polyphasic mixtures.[98] In addition to the structure determination of the framework, there is a large interest in locating templates or extra molecules hosted inside cavities[66,147] and in properly modeling the polytypic disorder in the framework.[54,58]

Metal–organic frameworks (MOFs),[21,56,62,66,68,112] covalent organic frameworks (COFs),[148] and hybrid layered compounds[149] are porous materials whose structures rely on organic linkers. They are generally developed to extend the typical pore size of conventional inorganic zeolites. In cases where single crystals could not be grown, 3D ED proved a robust protocol also for the structure investigation for such hybrid and organic compounds. All kinds of porous materials may suffer fast deterioration under the electron beam, but cooling the sample at liquid N_2 temperature[21,22,148] and collecting data in fast continuous mode[68,70,145] generally allow a complete and reliable data acquisition.

4.4. Aperiodic Materials. Aperiodic materials are a specific class of materials that exhibit long-range order but cannot be described within a 3D periodic system. Periodicity can be recovered by using a crystallographic description in a higher dimensional space.[150,151] Although not common, aperiodic structures appear in all classes of materials. In the most simple cases, incommensurately modulated phases have only one modulation vector, and only one extra dimension $(3 + 1)D$ is sufficient to describe their system. Their diffraction patterns combine strong "main" reflections related to the average cell with much weaker "satellite" reflections related to the periodic perturbation (the modulation), which can be found in irrational positions with respect to the average cell. This makes them very difficult to identify and to analyze when only powder diffraction data is available. For this reason, incommensurately modulated structures have been the subject of study by 3D ED methods from the early days.[23] Following this work, Boullay et al.[80] and Steciuk et al.[64,122] deduced the incommensurately modulated structures of several Aurivillius related compounds in the system $Bi_5Nb_3O_{15}–ABi_2Nb_2O_9$ (A = Ba, Sr, and Pb). Buixaderas et al.[52] analyzed the temperature-dependent structural changes of the tetragonal-tungsten–bronze type compound $Sr_{0.35}Ba_{0.69}Nb_2O_{6.04}$. Lanza et al.[74] determined and refined the natural modulated structure of the mineral daliranite

($PbHgAs_2S_5$). Recently the dynamical refinement was generalized to the case of modulated structures and applied to deduce the structure of $Hf_3Ta_2O_{11}$.[67]

Another level of complexity can be found in structures that need the application of a $(3 + 2)$D superspace. The first incommensurately modulated structure solved by 3D ED methods was actually the two-dimensionally modulated structure of tricopper silicide-germanide.[23] The same need applies to composite structures that can be seen as the imbrication of two distinct 3D average cells, whose coexistence induces a periodical perturbation of both systems. When stabilized in the form of thin films, such a system represents a challenge that only 3D ED can elucidate thanks to the possibility to map reciprocal space from nanosized areas.[152]

Lastly, quasicrystals are aperiodic materials characterized by the presence of forbidden rotational symmetries (5-, 8-, 10-, or 12-fold) that require the use of either $(3 + 2)$D or $(3 + 3)$D superspace groups and for which the structure determination from diffraction data is extremely rare. To date, no quasicrystalline material has been solved using 3D ED, but this method has been successfully applied for the study of 3D periodic "approximants" of quasicrystals.[110,153]

5. APPLICATIONS IN LIFE SCIENCES

In most current TEM applications to life sciences, the diffracted electrons are refocused into an image by the electromagnetic lenses. Recently, the method achieved spectacular breakthroughs culminating in the award of the 2017 Nobel Prize in Chemistry to Henderson, Frank, and Dubochet for the development of the cryo-EM method.[87,88] A remarkable advantage of cryo-EM is that frozen samples, vitrified at liquid nitrogen temperature, can be studied without the need of growing crystals and in their native, hydrated environment, while the low temperature reduces the effects of radiation damage.

The study of 2D protein crystals by directly measuring the diffracted intensities, i.e., by ED, was surely a scientific focus at the end of the past century.[154−156] Gonen et al.[12] were able to solve and refine AQP0 junctions at 1.9 Å resolution, and preliminary, low-resolution determinations of 3D structures were also attempted.[157] However, the structural study of proteins by electron diffraction lost most of its luster until recently, when 3D crystals definitely became the object of study.[36−45] Such renewed interest was fueled by technical developments and insights.

First, experimental evidence indicated that dynamical scattering affects ED data from 3D protein crystals to a far lesser extent[41,42] than anticipated by theoretical considerations.[158,159] Also, a significantly higher signal-to-noise ratio is expected in ED, as predicted by first principles calculations.[160] Thus, even when technology would allow the development of the ideal electron microscope, measuring in diffraction mode will still result in significantly better data. The improved signal comes at a price, though: the crystallographic phase information, which is lost in diffraction, has to be reconstructed a posteriori.

A biological or pharmaceutical sample can tolerate only a limited electron dose, before radiation damage destroys its functional structure.[161−163] This implies that data are limited by counting statistics. The advent of direct electron detectors[164] was essential for cryo-EM imaging. Such detectors have been successfully used also for ED,[49] but they are not always suited for measuring electron diffraction, because of their inadequate dynamic range and radiation hardness. On the other hand,

conventional detectors for ED, like CCD and CMOS, quantify electrons indirectly from the release of photons emitted when high-energy electrons hit a phosphor.

New-generation hybrid pixel detectors are more sensitive as their pixels count electrons directly and without readout noise.[29,33,36,96,165] These detectors are based on the charge separation within a semiconductor upon absorption of the full energy of the incident diffracted electrons. Hybrid pixel detectors can reach count rates higher than 10^8 electron hits per second per pixel, without readout noise. Their data accuracy is entirely determined by quantization—counting statistics—of the high-energy electrons, while their readout speed, of 1000 frames per second and higher, allows full data sets to be collected in just a handful of seconds. Hybrid detectors have recently become available commercially and are quickly becoming standard retrofits to existing TEMs in many electron crystallography laboratories.

Current applications of ED in life sciences are mainly found in the crystallographic structure determination of "small-molecule" organic compounds and proteins. Although peptides and proteins are both polyamino acids, from a crystallographic, methodological, and experimental perspective, peptides—and protein fragments in general—are closer to crystals of anhydrous organic compounds. In particular, peptides allow collecting diffraction data up to atomic resolution, and therefore, their structure determination can be often achieved ab initio by direct methods.

5.1. Small-Molecule Organic Compounds: Pharmaceuticals and Peptides.
Nowadays, different kinds of spectroscopic methods, and in particular NMR, allow an easy determination of the molecule connectivity for crystalline and noncrystalline organic materials. Still, many molecular compounds can pack into different polymorphic arrangements, which in turn have different physical, chemical, and therapeutic properties. A comprehensive structure determination, including polymorphism, requires therefore diffraction data, which are normally obtained by X-ray methods. In this perspective, 3D ED allows structure analysis of single, far smaller crystalline domains. This ability allows structure determination without the need for growing large coherent crystals, as required for X-ray diffraction, a procedure that may be time-consuming, complicated, or even fully unfeasible for certain pharmaceutical compounds or biological derivates.[31,32]

The main difficulty, when working with ED on organics, is that such compounds quickly get damaged by the electron beam. Cryo-plunging or just cooling the sample at liquid N_2 temperature is a common experimental procedure for slowing down the crystal deterioration induced by the electron beam.[31,32,46−50] On the other hand, when nano- or microcrystals of peptides and other organic compounds do not contain much disordered bulk solvent, their preservation in the vacuum of the microscope is relatively straightforward, and they can even be measured at ambient temperature if a sufficiently sensitive detector is available.[29,55] At any rate, continuous rotation 3D ED would be the method of choice for data acquisition to minimize the total electron dose on the sample.[36,38,40,89]

In addition to cryo-cooling, the limitations on data quality imposed by radiation sensitivity can be mitigated by the implementation of serial crystallography data collection strategies, in which many individual, static nanocrystals are illuminated to destruction.[53,109,166,167] A second way for lessening the drawback of beam damage is to diffract from somewhat larger crystals. This will partially compromise data
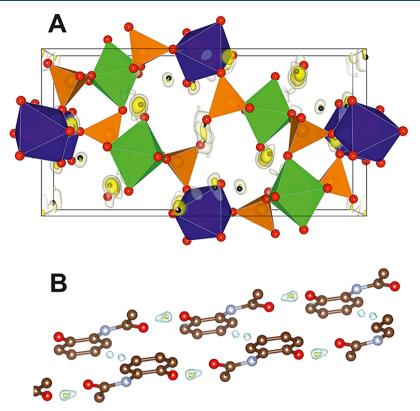
Figure 5. Hydrogen atoms localization by 3D ED. (A) Perspective view of the $Co_{1.13}Al_2P_4O_{20}H_{11.74}$ structure[105] with a superimposed difference potential map showing maxima at the positions of the hydrogen atoms. Isosurface levels are at $2\sigma[\Delta V(r)]$ (light gray) and $3\sigma[\Delta V(r)]$ (yellow). CoO_6, AlO_6, and PO_4 polyhedra are represented in blue, green, and orange, respectively, while oxygen atoms are in red. This difference potential map enlightening the hydrogen positions is obtained thanks to the use of dynamical refinement. The hydrogen positions (in black) are stable once incorporated to the dynamical refinement. (B) Two adjacent orthocetamol chains[34] with the superimposed difference Fourier map. The maximum residual potential (in blue and yellow) corresponds to the hydrogen atom responsible for the intermolecular bonding. Carbon atoms are drawn in brown, oxygen atoms in red, and nitrogen atoms in gray.

quality by increasing the dynamical scattering contribution, but for organics, such an effect only becomes important beyond a crystal thickness of about 100 nm.[24,160]

When data resolution is around 1 Å or better, phase determination can normally be obtained *ab initio* by direct methods.[29,31,32,34,35,47] In certain cases, even hydrogen atoms can be spotted directly in the potential map after *ab initio* phasing (Figure 5B)[34,46] or can be determined after treatment for dynamical effects.[35,105] If data to such a resolution are not available, global optimization methods like simulated annealing can be still successful, given the limitation that they rely on the *a priori* knowledge of the molecular compound.[55] 3D ED was already successfully employed for unveiling the structure of unknown pharmaceuticals[34] and protein fragments[46−49] that could not be addressed by X-ray methods because they could not be grown in large crystals, and in certain cases even for determining their absolute configuration.[73]

Dynamical diffraction will hamper proper structure refinement and validation. For very high-quality X-ray data of small organic molecular compounds, the refinement residual $R1$ can be as low as 2.5%, while samples with $R1$ values close to 5% and goodness-of-fit (GooF) values close to 1 are generally considered good. For ED data taken from crystals thicker than 100 nm, typical refinement statistics range from 18% to 40% in $R1$, and GooF ranges from 1.4 to 2.8.[31,32] These relatively poor statistics reveal significant inadequacies of the kinematical diffraction approximation, which prevents a confident validation of fine details in the atomic structures of unknown compounds.

Systematic deviations in the measured data due to dynamical diffraction can be reduced by including the effects of dynamical scattering in the crystal refinement. For instance, full unrestrained dynamical refinement of the paracetamol structure, based on 3D ED data taken from a 90 nm thick crystal, allowed a $R1$ of 9% and a GooF of 2.5.[105] A statistical correction for dynamical scattering allowed instead the refinement of $C_{16}O_5H_{18}$ and $C_{18}O_6N_2S_2H_{16}$ structures up to a $R1$ of 12% and a GooF of 0.9, starting from data collected on crystals with thicknesses of about 100−200 nm.[35] Both approaches were shown to be sensitive to hydrogen atom positions.

Hence, current approaches in 3D ED allow confident *ab initio* structure determination using single submicrometer crystals. Also, methods for dealing with the adverse effects of dynamical diffraction are now quickly progressing toward full and unrestrained refinement of hydrogen atoms and toward the reliable identification of atomic species, alternate and partial occupied positions, and anisotropic displacement parameters.

5.2. Proteins. Protein crystals contain 50% of disordered matter on average. Mostly, this is water located between the globular protein molecules, but crystals of membrane proteins also contain substantial amounts of disordered detergent. Moreover, water is volatile under the TEM vacuum, and its loss definitely compromises the crystallinity of the sample. Therefore, protein crystals must be vitrified and kept frozen to allow their study by cryo-EM or ED. Also, the relatively large unit cell, combined with a high amount of disordered volume,

> methods for dealing with the adverse effects of dynamical diffraction are now quickly progressing toward full and unrestrained refinement of hydrogen atoms and toward the reliable identification of atomic species, alternate and partial occupied positions, and anisotropic displacement parameters

compromises the resolution and intensity of the Bragg reflections of protein crystals.

Collecting diffraction data by rotating the crystal around a random axis normal to the beam has been the standard approach in X-ray protein crystallography over the past four decades.[168] All recent attempts to collect 3D ED data were then performed with a similar experimental setup. The continuous rotation method, where a series of diffraction patterns are collected while the crystal is continuously rotated between subsequent exposures, is the most common approach for ED data collection.[36,38,40] Recently Lanza et al.[45] showed that it is also possible to acquire data stepwise by a precession-assisted nanobeam, while crystal tracking is done in STEM imaging mode. The main advantage of employing a nanobeam is that a small portion of the crystal is illuminated per time, allowing the sampling of smaller features and exploiting more efficiently the protein diffracting volume.

The first protein structure successfully determined was the most common tetragonal polymorph of lysozyme.[37,38] Later, Gonen and co-workers also succeeded in the structure determination of a number of protein species, with resolution below 2.0 Å.[42] They also showed that is possible to obtain information about the binding interactions between a small-molecule inhibitor and the surrounding HIV-1 Gag.[43]

Meanwhile, Yonekura et al.[39] demonstrated the advantage of energy-filtering ED data for a better definition of charged amino acid residues and metals. Xu et al.[44] stressed the improvement in the potential map definition derived by data redundancy. Eventually Lanza et al.[45] reported a polymorphic form of lysozyme that was also independently discovered with powder X-ray diffraction[169] but could be solved only by 3D ED. The same authors also showed how 3D ED and microfocused X-ray diffraction can be coupled for following protein crystallogenesis and growth.

Protein crystals hardly ever diffract to a resolution that is sufficiently high for phasing by direct methods, so other phasing methods are required. Crystallographic phasing by imaging has been successful for two-dimensional,[156] but so far not for three-dimensional, protein crystals. To date, most proteins determined by 3D ED data are proteins whose crystal structure was known from previous X-ray analyses. This is related with the fact that, at present, there is no satisfactory way of determining the phases of protein ED data other than molecular replacement, which is a very robust phasing method when the atomic structure of a similar molecule is available. Still, independent validation methods are evidently required. A potential validation is obtained removing parts of the model and checking if difference Fourier mapping reveals residual density corresponding to the missing parts. Nevertheless, for this procedure it is essential that an independent model is used and that no refinement was done before the difference Fourier mapping.

Undoubtedly, unmodeled dynamical scattering contributes to reduce accuracy and worsen agreement factors. Protein structures are currently too complex for a full dynamical refinement,[101,102,105] but recently a statistical correction for estimating dynamical scattering has been proposed.[35] This procedure allows a small, but significant, improvement of the models. For instance, in the case of lysozyme nanocrystals, this statistical correction resulted in a reduction of $R_{complete}$ from 29% to 26%.[35,41]

We conclude that the electron diffraction of protein crystals may yield structural information that is almost as good as what can be achieved with X-ray diffraction, while requiring diffracted volumes that can be reduced by up to 6 orders of magnitude. However, several theoretical and experimental problems remain to be fully answered, and for general applications it will be indispensable to develop alternative phasing methods that do not rely on molecular replacement.

6. OUTLOOK

This paper outlines the strengths of electron crystallography for the analysis of nanocrystalline materials and the advances this technique experienced in the past decade. The impressive numbers of crystal structures determined by 3D ED in any domain of materials and life sciences testify to how advanced and powerful this method has become by now.

Robust and reliable protocols have been developed for ED data acquisition based on different approaches: sequential stage tilt with electron beam precession, combined stage-beam tilt, and continuous stage rotation. A common line for the data processing has been established using either dedicated programs for electron diffraction or modified X-ray packages. Most existing structure analysis and phase retrieval methods were successfully tested with 3D ED data. Meanwhile, the amount of structures characterized by 3D ED is continuously growing, including new complex material systems like proteins.

Taken together, 3D ED is rapidly gaining ground. The remaining steps concern the availability of dedicated instruments optimized for 3D ED. TEM is designed as imaging instruments, and their illumination systems and sample stages are not part of an electron diffractometer, which should provide 3D ED data on nanocrystals of any beam sensitivity. The mechanical stability of the sample stages should be improved to reduce the sample movement during tilt. The instruments should be equipped with single-electron detectors for diffraction, and the illumination system should provide parallel nanobeams smaller than 100 nm. The crystal search should be completely automatized with the possibility of performing ED in low dose conditions. Once such instruments will be available, 3D ED will be the gold standard every time the grain size goes beyond the micron size.

The overview that is provided in this Outlook aims to inform the research community beyond the current users of the method. Thereby, we encourage the outreach of 3D ED toward new materials and new scientific topics, and we foster cooperation among diverse research fields, such as materials and life sciences.

■ AUTHOR INFORMATION

Corresponding Author
*E-mail: mauro.gemmi@iit.it.

ORCID

Mauro Gemmi: 0000-0001-9542-3783

Philippe Boullay: 0000-0002-2867-8986

Notes

The authors declare no competing financial interest.

REFERENCES

(1) Belsky, A.; Hellenbrandt, M.; Karen, V. L.; Luksch, P. New developments in the Inorganic Crystal Structure Database (ICSD): accessibility in support of materials research and design. *Acta Crystallogr., Sect. B: Struct. Sci.* **2002**, *58*, 364−369.

(2) Downs, R. T.; Hall-Wallace, M. The *American Mineralogist* Crystal Structure Database. *Am. Mineral.* **2003**, *88*, 247−250.

(3) Gražulis, S.; Chateigner, D.; Downs, R. T.; Yokochi, A. F. T.; Quiros, M.; Lutterotti, L.; Manakova, E.; Butkus, J.; Moeck, P.; Le Bail, A. Crystallography Open Database − an open-access collection of crystal structures. *J. Appl. Crystallogr.* **2009**, *42*, 726−729.

(4) Groom, C. R.; Bruno, I. J.; Lightfoot, M. P.; Ward, S. C. The Cambridge Structural Database. *Acta Crystallogr., Sect. B: Struct. Sci., Cryst. Eng. Mater.* **2016**, *72*, 171−179.

(5) Burley, S. K.; Berman, H. M.; Bhikadiya, C.; Bi, C.; Chen, L.; Di Costanzo, L.; Christie, C.; Dalenberg, K.; Duarte, J. M.; Dutta, S.; Feng, Z.; Ghosh, S.; Goodsell, D. S.; Green, R. K.; Guranović, V.; Guzenko, D.; Hudson, B. P.; Kalro, T.; Liang, Y.; Lowe, R.; Namkoong, H.; Peisach, E.; Periskova, I.; Prlić, A.; Randle, C.; Rose, A.; Rose, P.; Sala, R.; Sekharan, M.; Shao, C.; Tan, L.; Tao, Y.-P.; Valasatava, Y.; Voigt, M.; Westbrook, J.; Woo, J.; Yang, H.; Young, J.; Zhuravleva, M.; Zardecki, C. RCSB Protein Data Bank: biological macromolecular structures enabling research and education in fundamental biology, biomedicine, biotechnology and energy. *Nucleic Acids Res.* **2019**, *47*, D464−D474.

(6) Cowley, J. M. *Electron diffraction techniques*; Oxford University Press: New York, 1992; Vols. *1 and 2*.

(7) Dorset, D. L. *Structural electron crystallography*; Plenum Pres: New York, 1995.

(8) Dorset, D. L.; Hauptman, H. A. Direct phase determination for quasi-kinematical electron diffraction intensity data from organic microcrystals. *Ultramicroscopy* **1976**, *1*, 195−201.

(9) Dorset, D. L. Electron crystallography. *Acta Crystallogr., Sect. B: Struct. Sci.* **1996**, *52*, 753−769.

(10) Weirich, T. E.; Ramlau, R.; Simon, A.; Hovmöller, S.; Zou, X. A crystal structure determined with 0.02 Å accuracy by electron microscopy. *Nature* **1996**, *382*, 144−146.

(11) Weirich, T. E.; Zou, X.; Ramlau, R.; Simon, A.; Cascarano, G. L.; Giacovazzo, C.; Hovmöller, S. Structures of nanometre-size crystals determined from selected-area electron diffraction data. *Acta Crystallogr., Sect. A: Found. Crystallogr.* **2000**, *56*, 29−35.

(12) Gonen, T.; Cheng, Y.; Sliz, P.; Hiroaki, Y.; Fujiyoshi, Y.; Harrison, S. C.; Walz, T. Lipid-protein interactions in double-layered two-dimensional AQP0 crystals. *Nature* **2005**, *438*, 633−638.

(13) Dorset, D. L.; Roth, W. J.; Gilmore, C. J. Electron crystallography of zeolites − the MWW family as a test of direct 3D structure determination. *Acta Crystallogr., Sect. A: Found. Crystallogr.* **2005**, *61*, 516−527.

(14) Gemmi, M.; Zou, X.; Hovmöller, S.; Migliori, A.; Vennström, M.; Andersson, Y. Structure of Ti2P solved by three-dimensional electron diffraction data collected with the precession technique and high-resolution electron microscopy. *Acta Crystallogr., Sect. A: Found. Crystallogr.* **2003**, *59*, 117−126.

(15) Kolb, U.; Gorelik, T.; Kübel, C.; Otten, M. T.; Hubert, D. Towards automated diffraction tomography: Part I—Data acquisition. *Ultramicroscopy* **2007**, *107*, 507−513.

(16) Kolb, U.; Gorelik, T.; Otten, M. T. Towards automated diffraction tomography. Part II—Cell parameter determination. *Ultramicroscopy* **2008**, *108*, 763−772.

(17) Mugnaioli, E.; Gorelik, T.; Kolb, U. Ab Initio" structure solution from electron diffraction data obtained by a combination of automated diffraction tomography and precession technique. *Ultramicroscopy* **2009**, *109*, 758−765.

(18) Kolb, U.; Mugnaioli, E.; Gorelik, T. E. Automated electron diffraction tomography − A new tool for nano crystal structure analysis. *Cryst. Res. Technol.* **2011**, *46*, 542−554.

(19) Birkel, C. S.; Mugnaioli, E.; Gorelik, T.; Kolb, U.; Panthöfer, M.; Tremel, W. Solution synthesis of a new thermoelectric Zn$_{1+x}$Sb nanophase and its structure determination using automated electron diffraction tomography. *J. Am. Chem. Soc.* **2010**, *132*, 9881−9889.

(20) Rozhdestvenskaya, I.; Mugnaioli, E.; Czank, M.; Depmeier, W.; Kolb, U.; Reinholdt, A.; Weirich, T. The structure of charoite, (K,Sr,Ba,Mn)$_{15−16}$(Ca,Na)$_{32}$[(Si$_{70}$(O,OH)$_{180}$)](OH,F)$_{4.0}$·nH$_2$O, solved by conventional and automated electron diffraction. *Mineral. Mag.* **2010**, *74*, 159−177.

(21) Denysenko, D.; Grzywa, M.; Tonigold, M.; Streppel, B.; Krkljus, I.; Hirscher, M.; Mugnaioli, E.; Kolb, U.; Hanss, J.; Volkmer, D. Elucidating gating effects for hydrogen sorption in MFU-4-type triazolate-based metal−organic frameworks featuring different pore sizes. *Chem. - Eur. J.* **2011**, *17*, 1837−1848.

(22) Jiang, J.; Jorda, J. L.; Yu, J.; Baumes, L. A.; Mugnaioli, E.; Diaz-Cabanas, M. J.; Kolb, U.; Corma, A. Synthesis and structure determination of the hierarchical meso-microporous zeolite ITQ-43. *Science* **2011**, *333*, 1131−1134.

(23) Palatinus, L.; Klementová, M.; Dřínek, V.; Jarošova, M.; Petříček, V. An incommensurately modulated structure of η′-phase of Cu$_{3+x}$Si determined by quantitative electron diffraction tomography. *Inorg. Chem.* **2011**, *50*, 3743−3751.

(24) Gorelik, T. E.; van de Streek, J.; Kilbinger, A. F. M.; Brunklaus, G.; Kolb, U. *Ab-initio* crystal structure analysis and refinement approaches of oligo *p*-benzamides based on electron diffraction data. *Acta Crystallogr., Sect. B: Struct. Sci.* **2012**, *68*, 171−181.

(25) Martínez-Franco, R.; Moliner, M.; Yun, Y.; Sun, J.; Wan, W.; Zou, X.; Corma, A. Synthesis of an extra-large molecular sieve using proton sponges as organic structure-directing agents. *Proc. Natl. Acad. Sci. U. S. A.* **2013**, *110*, 3749−3754.

(26) Förster, C.; Gorelik, T. E.; Kolb, U.; Ksenofontov, V.; Heinze, K. Crystalline non-equilibrium phase of a cobalt(II) complex with tridentate ligands. *Eur. J. Inorg. Chem.* **2015**, *2015*, 920−924.

(27) Guo, P.; Shin, J.; Greenaway, A. G.; Min, J. G.; Su, J.; Choi, H. J.; Liu, L.; Cox, P. A.; Hong, S. B.; Wright, P. A.; Zou, X. A Zeolite Family with expanding structural complexity and embedded isoreticular structures. *Nature* **2015**, *524*, 74−78.

(28) Zhang, W.; Li, M.; Chen, A.; Li, L.; Zhu, Y.; Xia, Z.; Lu, P.; Boullay, P.; Wu, L.; Zhu, Y.; MacManus-Driscoll, J. L.; Jia, Q.; Zhou, H.; Narayan, J.; Zhang, X.; Wang, H. Two-dimensional layered oxide structures tailored by self-assembled layer stacking via interfacial strain. *ACS Appl. Mater. Interfaces* **2016**, *8*, 16845−16851.

(29) van Genderen, E.; Clabbers, M. T. B.; Das, P. P.; Stewart, A.; Nederlof, I.; Barentsen, K. C.; Portillo, Q.; Pannu, N. S.; Nicolopoulos, S.; Gruene, T.; Abrahams, J. P. *Ab initio* structure determination of nanocrystals of organic pharmaceutical compounds by electron diffraction at room temperature using a Timepix quantum area direct electron detector. *Acta Crystallogr., Sect. A: Found. Adv.* **2016**, *72*, 236−242.

(30) Wang, Y.; Takki, S.; Cheung, O.; Xu, H.; Wan, W.; Öhrström, L.; Inge, A. K. Elucidation of the elusive structure and formula of the active pharmaceutical ingredient bismuth subgallate by continuous rotation electron diffraction. *Chem. Commun.* **2017**, *53*, 7018−7021.

(31) Gruene, T.; Wennmacher, J. T. C.; Zaubitzer, C.; Holstein, J. J.; Heidler, J.; Fecteau-Lefebvre, A.; De Carlo, S.; Müller, E.; Goldie, K. N.; Regeni, I.; Li, T.; Santiso-Quinones, G.; Steinfeld, G.; Handschin, S.;

van Genderen, E.; van Bokhoven, J. A.; Clever, G. H.; Pantelic, R. Rapid structure determination of microcrystalline molecular compounds using electron diffraction. *Angew. Chem., Int. Ed.* **2018**, *57*, 16313–16317.

(32) Jones, C. G.; Martynowycz, M. W.; Hattne, J.; Fulton, T. J.; Stoltz, B. M.; Rodriguez, J. A.; Nelson, H. M.; Gonen, T. The cryoEM method MicroED as a powerful tool for small molecule structure determination. *ACS Cent. Sci.* **2018**, *4*, 1587–1592.

(33) Tinti, G.; Fröjdh, E.; van Genderen, E.; Gruene, T.; Schmitt, B.; de Winter, D. A. M.; Weckhuysen, B. M.; Abrahams, J. P. Electron crystallography with the EIGER detector. *IUCrJ* **2018**, *5*, 190–199.

(34) Andrusenko, I.; Hamilton, V.; Mugnaioli, E.; Lanza, A.; Hall, C.; Potticary, J.; Hall, S. R.; Gemmi, M. The crystal structure of orthocetamol solved by 3D electron diffraction. *Angew. Chem., Int. Ed.* **2019**, in press. DOI: 10.1002/anie.201904564.

(35) Clabbers, M. T. B.; Gruene, T.; van Genderen, E.; Abrahams, J. P. Reducing dynamical electron scattering reveals hydrogen atoms. *Acta Crystallogr., Sect. A: Found. Adv.* **2019**, *75*, 82–93.

(36) Nederlof, I.; van Genderen, E.; Li, Y.-W.; Abrahams, J. P. A Medipix quantum area detector allows rotation electron diffraction data collection from submicrometre three-dimensional protein crystals. *Acta Crystallogr., Sect. D: Biol. Crystallogr.* **2013**, *69*, 1223–1230.

(37) Shi, D.; Nannenga, B. L.; Iadanza, M. G.; Gonen, T. Three-dimensional electron crystallography of protein microcrystals. *eLife* **2013**, *2*, No. e01345.

(38) Nannenga, B. L.; Shi, D.; Leslie, A. G. W.; Gonen, T. High-resolution structure determination by continuous-rotation data collection in MicroED. *Nat. Methods* **2014**, *11*, 927–930.

(39) Yonekura, K.; Kato, K.; Ogasawara, M.; Tomita, M.; Toyoshima, C. Electron crystallography of ultrathin 3D protein crystals: Atomic model with charges. *Proc. Natl. Acad. Sci. U. S. A.* **2015**, *112*, 3368–3373.

(40) Shi, D.; Nannenga, B. L.; De La Cruz, M. J.; Liu, J.; Sawtelle, S.; Calero, G.; Reyes, E. F.; Hattne, J.; Gonen, T. The collection of MicroED data for macromolecular crystallography. *Nat. Protoc.* **2016**, *11*, 895–904.

(41) Clabbers, M. T. B.; van Genderen, E.; Wan, W.; Wiegers, E. L.; Gruene, T.; Abrahams, J. P. Protein structure determination by electron diffraction using a single three-dimensional nanocrystal. *Acta Crystallogr. D* **2017**, *73*, 738–748.

(42) de la Cruz, M. J.; Hattne, J.; Shi, D.; Seidler, P.; Rodriguez, J.; Reyes, F. E.; Sawaya, M. R.; Cascio, D.; Weiss, S. C.; Kim, S. K.; Hinck, C. S.; Hinck, A. P.; Calero, G.; Eisenberg, D.; Gonen, T. Atomic-resolution structures from fragmented protein crystals with the cryoEM method MicroED. *Nat. Methods* **2017**, *14*, 399–402.

(43) Purdy, M. D.; Shi, D.; Chrustowicz, J.; Hattne, J.; Gonen, T.; Yeager, M. MicroED structures of HIV-1 Gag CTD-SP1 reveal binding interactions with the maturation inhibitor bevirimat. *Proc. Natl. Acad. Sci. U. S. A.* **2018**, *115*, 13258–13263.

(44) Xu, H.; Lebrette, H.; Yang, T.; Srinivas, V.; Hovmöller, S.; Högbom, M.; Zou, X. A rare lysozyme crystal form solved using highly redundant multiple electron diffraction datasets from micron-sized crystals. *Structure* **2018**, *26*, 667–675.

(45) Lanza, A.; Margheritis, E.; Mugnaioli, E.; Cappello, V.; Garau, G.; Gemmi, M. Nanobeam precession-assisted 3D electron diffraction reveals a new polymorph of hen egg-white lysozyme. *IUCrJ* **2019**, *6*, 178–188.

(46) Rodriguez, J. A.; Ivanova, M. I.; Sawaya, M. R.; Cascio, D.; Reyes, F. E.; Shi, D.; Sangwan, S.; Guenther, E. L.; Johnson, L. M.; Zhang, M.; Jiang, L.; Arbing, M. A.; Nannenga, B. L.; Hattne, J.; Whitelegge, J.; Brewster, A. S.; Messerschmidt, M.; Boutet, S.; Sauter, N. K.; Gonen, T.; Eisenberg, D. S. Structure of the toxic core of α-synuclein from invisible crystals. *Nature* **2015**, *525*, 486–490.

(47) Sawaya, M. R.; Rodriguez, J.; Cascio, D.; Collazo, M. J.; Shi, D.; Reyes, F. E.; Hattne, J.; Gonen, T.; Eisenberg, D. S. Ab initio structure determination from prion nanocrystals at atomic resolution by MicroED. *Proc. Natl. Acad. Sci. U. S. A.* **2016**, *113*, 11232–11236.

(48) Gallagher-Jones, M.; Glynn, C.; Boyer, D. R.; Martynowycz, M. W.; Hernandez, E.; Miao, J.; Zee, C.-T.; Novikova, I. V.; Goldschmidt, L.; McFarlane, H. T.; Helguera, G. F.; Evans, J. E.; Sawaya, M. R.; Cascio, D.; Eisenberg, D. S.; Gonen, T.; Rodriguez, J. A. Sub-ångström cryo-EM structure of a prion protofibril reveals a polar clasp. *Nat. Struct. Mol. Biol.* **2018**, *25*, 131–134.

(49) Guenther, E. L.; Ge, P.; Trinh, H.; Sawaya, M. R.; Cascio, D.; Boyer, D. R.; Gonen, T.; Zhou, Z. H.; Eisenberg, D. S. Atomic-level evidence for packing and positional amyloid polymorphism by segment from TDP-43 RRM2. *Nat. Struct. Mol. Biol.* **2018**, *25*, 311–319.

(50) Zee, C.-T.; Glynn, C.; Gallagher-Jones, M.; Miao, J.; Santiago, C. G.; Cascio, D.; Gonen, T.; Sawaya, M. R.; Rodriguez, J. A. Homochiral and racemic MicroED structures of a peptide repeat from the ice-nucleation protein InaZ. *IUCrJ* **2019**, *6*, 197–205.

(51) Bowden, D.; Krysiak, Y.; Palatinus, L.; Tsivoulas, D.; Plana-Ruiz, S.; Sarakinou, E.; Kolb, U.; Stewart, D.; Preuss, M. A high-strength silicide phase in a stainless steel alloy designed for wear-resistant applications. *Nat. Commun.* **2018**, *9*, 1374.

(52) Buixaderas, E.; Kempa, M.; Bovtun, V.; Kadlec, C.; Savinov, M.; Borodavka, F.; Vaněk, P.; Steciuk, G.; Palatinus, L.; Dec, J. Multiple polarization mechanisms across the ferroelectric phase transition of the tetragonal tungsten-bronze $Sr_{0.35}Ba_{0.69}Nb_2O_{6.04}$. *Physical Review Materials* **2018**, *2*, 124402.

(53) Cichocka, M. O.; Ångström, J.; Wang, B.; Zou, X.; Smeets, S. High-throughput continuous rotation electron diffraction data acquisition *via* software automation. *J. Appl. Crystallogr.* **2018**, *51*, 1652–1661.

(54) Cichocka, M. O.; Lorgouilloux, Y.; Smeets, S.; Su, J.; Wan, W.; Caullet, P.; Bats, N.; McCusker, L. B.; Paillaud, J.-L.; Zou, X. Multidimensional disorder in zeolite IM-18 revealed by combining transmission electron microscopy and X-ray powder diffraction analyses. *Cryst. Growth Des.* **2018**, *18*, 2441–2451.

(55) Das, P. P.; Mugnaioli, E.; Nicolopoulos, S.; Tossi, C.; Gemmi, M.; Galanis, A.; Borodi, G.; Pop, M. M. Crystal structures of two important pharmaceuticals solved by 3D precession electron diffraction tomography. *Org. Process Res. Dev.* **2018**, *22*, 1365–1372.

(56) Hynek, J.; Brázda, P.; Rohlíček, J.; Londesborough, M. G. S.; Demel, J. Phosphinic acid based linkers: Building blocks in metal–organic framework chemistry. *Angew. Chem., Int. Ed.* **2018**, *57*, 5016–5019.

(57) Karakulina, O. M.; Demortière, A.; Dachraoui, W.; Abakumov, A. M.; Hadermann, J. In situ electron diffraction tomography using a liquid-electrochemical transmission electron microscopy cell for crystal structure determination of cathode materials for Li-ion batteries. *Nano Lett.* **2018**, *18*, 6286–6291.

(58) Krysiak, Y.; Barton, B.; Marler, B.; Neder, R. B.; Kolb, U. *Ab initio* structure determination and quantitative disorder analysis on nano-particles by electron diffraction tomography. *Acta Crystallogr., Sect. A: Found. Adv.* **2018**, *74*, 93–101.

(59) Mayorga-Martinez, C. C.; Sofer, Z.; Luxa, J.; Huber, Š.; Sedmidubský, D.; Brázda, P.; Palatinus, L.; Mikulics, M.; Lazar, P.; Medlín, R.; Pumera, M. TaS₃ nanofibers: Layered trichalcogenide for high-performance electronic and sensing devices. *ACS Nano* **2018**, *12*, 464–473.

(60) Mugnaioli, E.; Gemmi, M.; Tu, R.; David, J.; Bertoni, G.; Gaspari, R.; De Trizio, L.; Manna, L. *Ab initio* structure determination of $Cu_{2−x}Te$ plasmonic nanocrystals by precession-assisted electron diffraction tomography and HAADF-STEM imaging. *Inorg. Chem.* **2018**, *57*, 10241–10248.

(61) Németh, P.; Mugnaioli, E.; Gemmi, M.; Czuppon, G.; Demény, A.; Spötl, C. A nanocrystalline monoclinic $CaCO_3$ precursor of metastable aragonite. *Sci. Adv.* **2018**, *4*, No. eaau6178.

(62) Portolés-Gil, N.; Lanza, A.; Aliaga-Alcalde, N.; Ayllón, J. A.; Gemmi, M.; Mugnaioli, E.; López-Periago, A. M.; Domingo, C. Crystalline curcumin bioMOF obtained by precipitation in supercritical CO_2 and structural determination by electron diffraction tomography. *ACS Sustainable Chem. Eng.* **2018**, *6*, 12309–12319.

(63) Seo, S.; Yang, T.; Shin, J.; Jo, D.; Zou, X.; Hong, S. B. Two aluminophosphate molecular sieves built from pairs of enantiomeric structural building units. *Angew. Chem., Int. Ed.* **2018**, *57*, 3727–3732.

(64) Steciuk, G.; Barrier, N.; Pautrat, A.; Boullay, P. Stairlike Aurivillius Phases in the pseudobinary $Bi_5Nb_3O_{15}$–$ABi_2Nb_2O_9$ (A = Ba and Sr) system: A comprehensive analysis using superspace group formalism. *Inorg. Chem.* **2018**, *57*, 3107–3115.

(65) Veis, M.; Minár, J.; Steciuk, G.; Palatinus, L.; Rinaldi, C.; Cantoni, M.; Kriegner, D.; Tikuišis, K. K.; Hamrle, J.; Zahradník, M.; Antoš, R.; Železný, J.; Šmejkal, L.; Marti, X.; Wadley, P.; Campion, R. P.; Frontera, C.; Uhlířová, K.; Duchoň, T.; Kužel, P.; Novák, V.; Jungwirth, T.; Výborný, K. Band structure of CuMnAs probed by optical and photoemission spectroscopy. *Phys. Rev. B: Condens. Matter Mater. Phys.* **2018**, *97*, 125109.

(66) Wang, B.; Rhauderwiek, T.; Inge, A. K.; Xu, H.; Yang, T.; Huang, Z.; Stock, N.; Zou, X. A porous cobalt tetraphosphonate metal–organic framework: Accurate structure and guest molecule location determined by continuous-rotation electron diffraction. *Chem. - Eur. J.* **2018**, *24*, 17429–17433.

(67) Wiedemann, D.; Lüdtke, T.; Palatinus, L.; Willinger, E.; Willinger, M. G.; Mühlbauer, M. J.; Lerch, M. At the Gates: The tantalum-rich phase $Hf_3Ta_2O_{11}$ and its commensurately modulated structure. *Inorg. Chem.* **2018**, *57*, 14435–14442.

(68) Yuan, S.; Qin, J.-S.; Xu, H.-Q.; Su, J.; Rossi, D.; Chen, Y.; Zhang, L.; Lollar, C.; Wang, Q.; Jiang, H.-L.; Son, D. H.; Xu, H.; Huang, Z.; Zou, X.; Zhou, H.-C. $[Ti_8Zr_2O_{12}(COO)_{16}]$ cluster: An ideal inorganic building unit for photoactive metal–organic frameworks. *ACS Cent. Sci.* **2018**, *4*, 105–111.

(69) Zacharias, N.; Karavassili, F.; Das, P.; Nicolopoulos, S.; Oikonomou, A.; Galanis, A.; Rauch, E.; Arenal, R.; Portillo, J.; Roque, J.; Casablanca, J.; Margiolaki, I. A novelty for cultural heritage material analysis: transmission electron microscope (TEM) 3D electron diffraction tomography applied to Roman glass tesserae. *Microchem. J.* **2018**, *138*, 19–25.

(70) Zhang, C.; Kapaca, E.; Li, J.; Liu, Y.; Yi, X.; Zheng, A.; Zou, X.; Jiang, J.; Yu, J. An extra-large-pore zeolite with 24 × 8 × 8-ring channels using a structure-directing agent derived from traditional Chinese medicine. *Angew. Chem., Int. Ed.* **2018**, *57*, 6486–6490.

(71) Zhou, Z.; Qiu, Y.; Liang, F.; Palatinus, L.; Poupon, M.; Yang, T.; Cong, R.; Lin, Z.; Sun, J. $CsSiB_3O_7$: A beryllium-free deep-ultraviolet nonlinear optical material discovered by the combination of electron diffraction and first-principles calculations. *Chem. Mater.* **2018**, *30*, 2203–2207.

(72) Ångström, J.; Jenei, I. Z.; Spektor, K.; Häussermann, U. Formation of hydrous, pyroxene-related phases from $LiAlSiO_4$ glass in high-pressure hydrothermal environments. *ACS Earth Space Chem.* **2019**, *3*, 8–16.

(73) Brázda, P.; Palatinus, L.; Babor, M. Electron diffraction determines molecular absolute configuration in a pharmaceutical nanocrystal. *Science* **2019**, *364*, 667–669.

(74) Lanza, A. E.; Gemmi, M.; Bindi, L.; Mugnaioli, E.; Paar, W. H. Daliranite, $PbHgAs_2S_5$: determination of the incommensurately modulated structure and revision of the chemical formula. *Acta Crystallogr. B* **2019**, in press. DOI: 10.1107/S2052520619007340.

(75) Rondeau, B.; Devouard, B.; Jacob, D.; Roussel, J.; Stephant, N.; Boulet, C.; Mollé, V.; Corre, M.; Fritsch, E.; Ferraris, C.; Parodi, G. C. Lasnierite, $(Ca,Sr)(Mg,Fe)_2Al(PO_4)_3$, a new phosphate accompanying lazulite from Mt. Ibity, Madagascar: an example of structural characterization from dynamical refinement of precession electron diffraction data on submicrometre sample. *Eur. J. Mineral.* **2019**, *31*, 379–388.

(76) Steciuk, G.; David, A.; Petricek, V.; Palatinus, L.; Mercey, B.; Prellier, W.; Pautrat, A.; Boullay, P. Precession electron diffraction tomography on twinned crystals: Application to $CaTiO_3$ thin films. *J. Appl. Crystallogr.* **2019**, *52*, 626–636.

(77) Zou, Z.; Habraken, W. J. E. M.; Matveeva, G.; Jensen, A. C. S.; Bertinetti, L.; Hood, M. A.; Sun, C.; Gilbert, P. U. P. A.; Polishchuk, I.; Pokroy, B.; Mahamid, J.; Politi, Y.; Weiner, S.; Werner, P.; Bette, S.; Dinnebier, R.; Kolb, U.; Zolotoyabko, E.; Fratzl, P. A hydrated crystalline calcium carbonate phase: Calcium carbonate hemihydrate. *Science* **2019**, *363*, 396–400.

(78) Hand, E.; Vogel, G.; Garber, K.; Kaiser, J.; Servick, K.; Clery, D.; Service, R. F.; Wadman, M. Runners-up. *Science* **2018**, *362*, 1346–1351.

(79) Gemmi, M.; Oleynikov, P. Scanning reciprocal space for solving unknown structures: energy filtered diffraction tomography and rotation diffraction tomography methods. *Z. Kristallogr. - Cryst. Mater.* **2013**, *228*, 51–58.

(80) Boullay, P.; Palatinus, L.; Barrier, N. Precession electron diffraction tomography for solving complex modulated structures: The case of $Bi_5Nb_3O_{15}$. *Inorg. Chem.* **2013**, *52*, 6127–6135.

(81) Zhang, D.; Oleynikov, P.; Hovmöller, S.; Zou, X. Collecting 3D electron diffraction data by the rotation method. *Z. Kristallogr.* **2010**, *225*, 94–102.

(82) Wan, W.; Sun, J.; Su, J.; Hovmöller, S.; Zou, X. Three-dimensional rotation electron diffraction: software *RED* for automated data collection and data processing. *J. Appl. Crystallogr.* **2013**, *46*, 1863–1873.

(83) Palatinus, L.; Chapuis, G. *SUPERFLIP* – a computer program for the solution of crystal structures by charge flipping in arbitrary dimensions. *J. Appl. Crystallogr.* **2007**, *40*, 786–790.

(84) Sheldrick, G. M. A short history of *SHELX*. *Acta Crystallogr., Sect. A: Found. Crystallogr.* **2008**, *64*, 112–122.

(85) Burla, M. C.; Caliandro, R.; Carrozzini, B.; Cascarano, G. L.; Cuocci, C.; Giacovazzo, C.; Mallamo, M.; Mazzone, A.; Polidori, G. Crystal structure determination and refinement *via* SIR2014. *J. Appl. Crystallogr.* **2015**, *48*, 306–309.

(86) Grimes, J. M.; Hall, D. R.; Ashton, A. W.; Evans, G.; Owen, R. L.; Wagner, A.; McAuley, K. E.; von Delft, F.; Orville, A. M.; Sorensen, T.; Walsh, M. A.; Ginn, H. M.; Stuart, D. I. Where is crystallography going? *Acta Crystallogr. D* **2018**, *74*, 152–166.

(87) Amunts, A.; Brown, A.; Bai, X.-C.; Llácer, J. L.; Hussain, T.; Emsley, P.; Long, F.; Murshudov, G.; Scheres, S. H. W.; Ramakrishnan, V. Structure of the yeast mitochondrial large ribosomal subunit. *Science* **2014**, *343*, 1485–1489.

(88) Cheng, Y. Single-particle cryo-EM at crystallographic resolution. *Cell* **2015**, *161*, 450–457.

(89) Gemmi, M.; La Placa, M. G. I.; Galanis, A. S.; Rauch, E. F.; Nicolopoulos, S. Fast electron diffraction tomography. *J. Appl. Crystallogr.* **2015**, *48*, 718–727.

(90) Vincent, R.; Midgley, P. A. Double conical beam-rocking system for measurement of integrated electron diffraction intensities. *Ultramicroscopy* **1994**, *53*, 271–282.

(91) Plana-Ruiz, S.; Portillo, J.; Estradé, S.; Peiró, F.; Kolb, U.; Nicolopoulos, S. Quasi-parallel precession diffraction: Alignment method for scanning transmission electron microscopes. *Ultramicroscopy* **2018**, *193*, 39–51.

(92) Gemmi, M.; Merlini, M.; Palatinus, L.; Fumagalli, P.; Hanfland, M. Electron diffraction determination of 11.5 Å and HySo structures: Candidate water carriers to the Upper Mantle. *Am. Am. Mineral.* **2016**, *101*, 2645–2654.

(93) Wilke, M.; Kabelitz, A.; Gorelik, T. E.; Guilherme Buzanich, A.; Reinholz, U.; Kolb, U.; Rademann, K.; Emmerling, F. The crystallisation of copper(II) phenylphosphonates. *Dalton T.* **2016**, *45*, 17453–17463.

(94) Rozhdestvenskaya, I. V.; Mugnaioli, E.; Schowalter, M.; Schmidt, M. U.; Czank, M.; Depmeier, W.; Rosenauer, A. The structure of denisovite, a fibrous nanocrystalline polytypic disordered 'very complex' silicate, studied by a synergistic multi-disciplinary approach employing methods of electron crystallography and X-ray powder diffraction. *IUCrJ* **2017**, *4*, 223–242.

(95) Mugnaioli, E.; Gemmi, M. Single-crystal analysis of nanodomains by electron diffraction tomography: mineralogy at the order-disorder borderline. *Z. Kristallogr. - Cryst. Mater.* **2018**, *233*, 163–178.

(96) Georgieva, D.; Jansen, J.; Sikharulidze, I.; Jiang, L.; Zandbergen, H. W.; Abrahams, J. P. Evaluation of Medipix2 detector for recording electron diffraction data in low dose conditions. *J. Instrum.* **2011**, *6*, C01033.

(97) Kodjikian, S.; Klein, H. Low-dose electron diffraction tomography (LD-EDT). *Ultramicroscopy* **2019**, *200*, 12–19.

(98) Yun, Y.; Wan, W.; Rabbani, F.; Su, J.; Xu, H.; Hovmöller, S.; Johnsson, M.; Zou, X. Phase identification and structure determination from multiphase crystalline powder samples by rotation electron diffraction. *J. Appl. Crystallogr.* **2014**, *47*, 2048−2054.

(99) Clabbers, M. T. B.; Gruene, T.; Parkhurst, J. M.; Abrahams, J. P.; Waterman, D. G. Electron diffraction data processing with *DIALS. Acta Cryst. D* **2018**, *74*, 506−518.

(100) Nannenga, B. L.; Shi, D.; Hattne, J.; Reyes, F. E.; Gonen, T. Structure of catalase determined by MicroED. *eLife* **2014**, *3*, No. e03600.

(101) Palatinus, L.; Petříček, V.; Antunes Corrêa, C. Structure refinement using precession electron diffraction tomography and dynamical diffraction: theory and implementation. *Acta Crystallogr., Sect. A: Found. Adv.* **2015**, *71*, 235−244.

(102) Palatinus, L.; Corrêa, C. A.; Steciuk, G.; Jacob, D.; Roussel, P.; Boullay, P.; Klemantová, M.; Gemmi, M.; Kopeček, J.; Domeneghetti, M. C.; Cámara, F.; Petříček, V. Structure refinement using precession electron diffraction tomography and dynamical diffraction: Tests on experimental data. *Acta Crystallogr., Sect. B: Struct. Sci., Cryst. Eng. Mater.* **2015**, *71*, 740−751.

(103) Hirsch, P.; Howie, A.; Nicholson, R.; Pashley, D.; Whelan, M. *Electron microscopy of thin crystals*; Robert E. Krieger: Malabar, FL, 1977.

(104) Zuo, J. M.; Spence, J. C. H. Automated structure factor refinement from convergent-beam patterns. *Ultramicroscopy* **1991**, *35*, 185−186.

(105) Palatinus, L.; Brázda, P.; Boullay, P.; Perez, O.; Klementová, M.; Petit, S.; Eigner, V.; Zaarour, M.; Mintova, S. Hydrogen positions in single nanocrystals revealed by electron diffraction. *Science* **2017**, *355*, 166−169.

(106) Klementová, M.; Karlík, M.; Novák, P.; Palatinus, P. Structure determination of a new phase Ni_8Ti_5 by electron diffraction tomography. *Intermetallics* **2017**, *85*, 110−116.

(107) Gonano, B.; Breard, Y.; Pelloquin, D.; Caignaert, V.; Perez, O.; Pautrat, A.; Boullay, P.; Bazin, P.; Le Breton, J. M. Combining multiscale approaches for the structure determination of an iron layered oxysulfate: $Sr_4Fe_{2.5}O_{7.25}(SO_4)_{0.5}$. *Inorg. Chem.* **2017**, *56*, 15241−15250.

(108) Klementová, M.; Motlochová, M.; Boháček, J.; Kupčík, J.; Palatinus, L.; Pližingrová, E.; Szatmáry, L.; Šubrt, J. Metatitanic acid pseudomorphs after titanyl sulfates: nanostructured sorbents and precursors for crystalline titania with desired particle size and shape. *Cryst. Growth Des.* **2017**, *17*, 6762−6769.

(109) de la Cruz, M. J.; Martynowycz, M. W.; Hattne, J.; Gonen, T. MicroED data collection with SerialEM. *Ultramicroscopy* **2019**, *201*, 77−80.

(110) Samuha, S.; Mugnaioli, E.; Grushko, B.; Kolb, U.; Meshi, L. Atomic structure solution of the complex quasicrystal approximant $Al_{77}Rh_{15}Ru_8$ from electron diffraction data. *Acta Crystallogr., Sect. B: Struct. Sci., Cryst. Eng. Mater.* **2014**, *70*, 999−1005.

(111) Drozhzhin, O. A.; Sumanov, V. D.; Karakulina, O. M.; Abakumov, A. M.; Hadermann, J.; Baranov, A. N.; Stevenson, K. J.; Antipov, E. V. Switching between solid solution and two-phase regimes in the $Li_{1-x}Fe_{1-y}Mn_yPO_4$ cathode materials during lithium (de)-insertion: combined PITT, in situ XRPD and electron diffraction tomography study *Electrochim. Electrochim. Acta* **2016**, *191*, 149−157.

(112) Feyand, M.; Mugnaioli, E.; Vermoortele, F.; Bueken, B.; Dieterich, J. M.; Reimer, T.; Kolb, U.; de Vos, D.; Stock, N. Automated diffraction tomography for the structure elucidation of twinned, sub-micrometer crystals of a highly porous, catalytically active bismuth metal−organic framework. *Angew. Chem., Int. Ed.* **2012**, *51*, 10373−10376.

(113) Brázda, P.; Palatinus, L.; Drahokoupil, J.; Knížek, K.; Buršík, J. Calcium-induced cation ordering and large resistivity decrease in $Pr_{0.3}CoO_2$. *J. Phys. Chem. Solids* **2016**, *96*−*97*, 10−16.

(114) Neagu, A.; Tai, C.-W. Local disorder in $Na_{0.5}Bi_{0.5}TiO_3$-piezoceramic determined by 3D electron diffuse scattering. *Sci. Rep.* **2017**, *7*, 12519.

(115) Zhao, H.; Krysiak, Y.; Hoffmann, K.; Barton, B.; Molina-Luna, L.; Neder, R. B.; Kleebe, H.-J.; Gesing, T. M.; Schneider, H.; Fischer, R.

X.; Kolb, U. Elucidating structural order and disorder phenomena in mullite-type $Al_4B_2O_9$ by automated electron diffraction tomography. *J. Solid State Chem.* **2017**, *249*, 114−123.

(116) Willhammar, T.; Sentosun, K.; Mourdikoudis, S.; Goris, B.; Kurttepeli, M.; Bercx, M.; Lamoen, D.; Partoens, B.; Pastoriza-Santos, I.; Pérez-Juste, J.; Liz-Marzán, L. M.; Bals, S.; Van Tendeloo, G. Structure and vacancy distribution in copper telluride nanoparticles influence plasmonic activity in the near-infrared. *Nat. Commun.* **2017**, *8*, 14925.

(117) Baraldi, A.; Buffagni, E.; Capelletti, R.; Mazzera, M.; Fasoli, M.; Lauria, A.; Moretti, F.; Vedda, A.; Gemmi, M. Eu incorporation into sol−gel silica for photonic applications: Spectroscopic and TEM evidences of α-quartz and Eu pyrosilicate nanocrystal growth. *J. Phys. Chem. C* **2013**, *117*, 26831−26848.

(118) Mayence, A.; Wang, D.; Salaz-Alvarez, G.; Oleynikov, P.; Bergström, L. Probing planar defects in nanoparticle superlattices by 3D small-angle electron diffraction tomography and real space imaging. *Nanoscale* **2014**, *6*, 13803−13808.

(119) Colmont, M.; Palatinus, L.; Huvé, M.; Kabbour, H.; Saitzek, S.; Djelal, N.; Roussel, P. On the use of dynamical diffraction theory to refine crystal structure from electron diffraction data: Application to $KLa_5O_5(VO_4)_2$, a material with promising luminescent properties. *Inorg. Chem.* **2016**, *55*, 2252−2260.

(120) Lepoittevin, C. Structure resolution by electron diffraction tomography of the complex layered iron-rich Fe-2234-type $Sr_5Fe_6O_{15.4}$. *J. J. Solid State Chem.* **2016**, *242*, 228−235.

(121) Rickert, K.; Boullay, P.; Malo, S.; Caignaert, V.; Poeppelmeier, K. R. A rutile chevron modulation in delafossite-like $Ga_{3-x}In_3Ti_xO_{9-x/2}$. *Inorg. Chem.* **2016**, *55*, 4403−4409.

(122) Steciuk, G.; Boullay, P.; Pautrat, A.; Barrier, N.; Caignaert, V.; Palatinus, L. Unusual relaxor ferroelectric behavior in stairlike aurivillius phases. *Inorg. Chem.* **2016**, *55*, 8881−8891.

(123) David, J.; Rossella, F.; Rocci, M.; Ercolani, D.; Sorba, L.; Beltram, F.; Gemmi, M.; Roddaro, S. Crystal phases in hybrid metal−semiconductor nanowire devices. *Nano Lett.* **2017**, *17*, 2336−2341.

(124) Mugnaioli, E.; Gemmi, M.; Merlini, M.; Gregorkiewitz, M. $(Na,)_5[MnO_2]_{13}$ nanorods: a new tunnel structure for electrode materials determined *ab initio* and refined through a combination of electron and synchrotron diffraction data. *Acta Crystallogr., Sect. B: Struct. Sci., Cryst. Eng. Mater.* **2016**, *72*, 893−903.

(125) Rotella, H.; Copie, O.; Steciuk, G.; Ouerdane, H.; Boullay, P.; Roussel, P.; Morales, M.; David, A.; Pautrat, A.; Mercey, B.; Lutterotti, L.; Chateigner, D.; Prellier, W. Structural analysis of strained $LaVO_3$ thin films. *J. Phys.: Condens. Matter* **2015**, *27*, 175001.

(126) Bhat, S.; Wiehl, L.; Molina-Luna, L.; Mugnaioli, E.; Lauterbach, S.; Sicolo, S.; Kroll, P.; Duerrschnabel, M.; Nishiyama, N.; Kolb, U.; Albe, K.; Kleebe, H.-J.; Riedel, R. High-pressure synthesis of novel boron oxynitride $B_6N_4O_3$ with sphalerite type structure. *Chem. Mater.* **2015**, *27*, 5907−5914.

(127) Lepoittevin, C.; Jeanneau, J.; Toulemonde, P.; Sulpice, A.; Núñez-Regueiro, M. $Ba_{19}Cr_{12}O_{45}$: A high pressure chromate with an original structure solved by electron diffraction tomography and powder X-ray diffraction. *Inorg. Chem.* **2017**, *56*, 6404−6409.

(128) Andrusenko, I.; Mugnaioli, E.; Gorelik, T. E.; Koll, D.; Panthöfer, M.; Tremel, W.; Kolb, U. Structure analysis of titanate nanorods by automated electron diffraction tomography. *Acta Crystallogr., Sect. B: Struct. Sci.* **2011**, *67*, 218−225.

(129) Weber, D.; Huber, M.; Gorelik, T. E.; Abakumov, A. M.; Becker, N.; Niehaus, O.; Schwickert, C.; Culver, S. P.; Boysen, H.; Senyshyn, A.; Pöttgen, R.; Dronskowski, R.; Ressler, T.; Kolb, U.; Lerch, M. Molybdenum oxide nitrides of the $Mo_2(O,N,\square)_5$ type: On the way to Mo_2O_5. *Inorg. Chem.* **2017**, *56*, 8782−8792.

(130) Gemmi, M.; Campostrini, I.; Demartin, F.; Gorelik, T. E.; Gramaccioli, C. M. Structure of the new mineral sarrabusite, $Pb_5CuCl_4(SeO_3)_4$, solved by manual electron-diffraction tomography. *Acta Crystallogr., Sect. B: Struct. Sci.* **2012**, *68*, 15−23.

(131) Plášil, J.; Palatinus, L.; Rohlíček, J.; Houdková, L.; Klementová, M.; Goliáš, V.; Škácha, P. Crystal structure of lead uranyl carbonate

mineral widenmannite: Precession electron-diffraction and synchrotron powder-diffraction study. *Am. Mineral.* **2014**, *99*, 276−282.

(132) Majzlan, J.; Palatinus, L.; Plášil, J. Crystal structure of $Fe_2(AsO_4)(HAsO_4)(OH)(H_2O)_3$, a dehydration product of kaňkite. *Eur. J. Mineral.* **2016**, *28*, 63−70.

(133) Colombo, F.; Mugnaioli, E.; Vallcorba, O.; Garcia, A.; Goñi, A. R.; Rius, J. Crystal structure determination of karibibite, an Fe^{3+} arsenite, using electron diffraction tomography. *Mineral. Mag.* **2017**, *81*, 1191−1202.

(134) Capitani, G. C.; Mugnaioli, E.; Rius, J.; Gentile, P.; Catelani, T.; Lucotti, A.; Kolb, U. The Bi sulfates from the Alfenza Mine, Crodo, Italy: An automatic electron diffraction tomography (ADT) study. *Am. Mineral.* **2014**, *99*, 500−510.

(135) Mugnaioli, E.; Reyes-Gasga, J.; Kolb, U.; Hemmerlé, J.; Brès, É. F. Evidence of noncentrosymmetry of human tooth hydroxyapatite crystals. *Chem. - Eur. J.* **2014**, *20*, 6849−6852.

(136) Capitani, G. C.; Mugnaioli, E.; Guastoni, A. What is the actual structure of samarskite-(Y)? A TEM investigation of metamict samarskite from the Garnet Codera dike pegmatite (Central Italian Alps). *Am. Mineral.* **2016**, *101*, 1679−1690.

(137) Mugnaioli, E.; Andrusenko, I.; Schüler, T.; Loges, N.; Dinnebier, R. E.; Panthöfer, M.; Tremel, W.; Kolb, U. Ab initio structure determination of vaterite by automated electron diffraction. *Angew. Chem., Int. Ed.* **2012**, *51*, 7041−7045.

(138) Pignatelli, I.; Marrocchi, Y.; Mugnaioli, E.; Bourdelle, F.; Gounelle, M. Mineralogical, crystallographic and redox features of the earliest stages of fluid alteration in CM chondrites. *Geochim. Cosmochim. Acta* **2017**, *209*, 106−122.

(139) Viti, C.; Brogi, A.; Liotta, D.; Mugnaioli, E.; Spiess, R.; Dini, A.; Zucchi, M.; Vannuccini, G. Seismic slip recorded in tourmaline fault mirrors from Elba Island (Italy). *J. Struct. Geol.* **2016**, *86*, 1−12.

(140) Gemmi, M.; Fischer, J.; Merlini, M.; Poli, S.; Fumagalli, P.; Mugnaioli, E.; Kolb, U. A new hydrous Al-bearing pyroxene as a water carrier in subduction zones. *Earth Planet. Sci. Lett.* **2011**, *310*, 422−428.

(141) Pignatelli, I.; Mugnaioli, E.; Hybler, J.; Mosser-Ruck, R.; Cathelineau, M.; Michau, N. A multi-technique characterization of cronstedtite synthesized by iron-clay interaction in a step-by-step cooling procedure. *Clays Clay Miner.* **2013**, *61*, 277−289.

(142) Koch-Müller, M.; Mugnaioli, E.; Rhede, D.; Speziale, S.; Kolb, U.; Wirth, R. Synthesis of a quenchable high-pressure form of magnetite $(h-Fe_3O_4)$ with composition $^{Fe1}(Fe^{2+}{}_{0.75}Mg_{0.26})^{Fe2}(Fe^{3+}{}_{0.70}Cr_{0.15}Al_{0.11}Si_{0.04})_2O_4$. *Am. Mineral.* **2014**, *99*, 2405−2415.

(143) Willhammar, T.; Burton, A. W.; Yun, Y.; Sun, J.; Afeworki, M.; Strohmaier, K. G.; Vroman, H.; Zou, X. EMM-23: A stable high-silica multidimensional zeolite with extra-large trilobe-shaped channels. *J. Am. Chem. Soc.* **2014**, *136*, 13570−13573.

(144) Jiang, J.; Yun, Y.; Zou, X.; Jorda, J. L.; Corma, A. ITQ-54: a multi-dimensional extra-large pore zeolite with $20 \times 14 \times 12$-ring channels. *Chem. Sci.* **2015**, *6*, 480−485.

(145) Simancas, J.; Simancas, R.; Bereciartua, P. J.; Jorda, J. L.; Rey, F.; Corma, A.; Nicolopoulos, S.; Das, P. P.; Gemmi, M.; Mugnaioli, E. Ultrafast electron diffraction tomography for structure determination of the new zeolite ITQ-58. *J. Am. Chem. Soc.* **2016**, *138*, 10116−10119.

(146) Willhammar, T.; Su, J.; Yun, Y.; Zou, X.; Afeworki, M.; Weston, S. C.; Vroman, H. B.; Lonergan, W. W.; Strohmaier, K. G. High-throughput synthesis and structure of zeolite ZSM-43 with two-directional 8-ring channels. *Inorg. Chem.* **2017**, *56*, 8856−8864.

(147) Rius, J.; Mugnaioli, E.; Vallcorba, O.; Kolb, U. Application of δ recycling to electron automated diffraction tomography data from inorganic crystalline nanovolumes. *Acta Crystallogr., Sect. A: Found. Crystallogr.* **2013**, *69*, 396−407.

(148) Zhang, Y.-B.; Su, J.; Furukawa, H.; Yun, Y.; Gándara, F.; Duong, A.; Zou, X.; Yaghi, O. M. Single-crystal structure of a covalent organic framework. *J. Am. Chem. Soc.* **2013**, *135*, 16336−16339.

(149) Bellussi, G.; Montanari, E.; Di Paola, E.; Millini, R.; Carati, A.; Rizzo, C.; O'Neil Parker, W., Jr.; Gemmi, M.; Mugnaioli, E.; Kolb, U.; Zanardi, S. ECS-3: a crystalline hybrid organic−inorganic aluminosilicate with open porosity. *Angew. Chem., Int. Ed.* **2012**, *51*, 666−669.

(150) Janssen, T.; Chapuis, G.; de Boissieu, M. *Aperiodic Crystals: from modulated phases to quasicrystals*; Oxford University Press: New York, 2007.

(151) van Smaalen, S. *Incommensurate crystallography*; Oxford University Press: New York, 2007.

(152) Li, L.; Boullay, P.; Lu, P.; Wang, X.; Jian, J.; Huang, J.; Gao, X.; Misra, S.; Zhang, W.; Perez, O.; Steciuk, G.; Chen, A.; Zhang, X.; Wang, H. Novel layered supercell structure from Bi_2AlMnO_6 for multifunctionalities. *Nano Lett.* **2017**, *17*, 6575−6582.

(153) Singh, D.; Yun, Y.; Wan, W.; Grushko, B.; Zou, X.; Hovmöller, S. A complex pseudo-decagonal quasicrystal approximant, $Al_{37}(Co,Ni)_{15.5}$, solved by rotation electron diffraction. *J. Appl. Crystallogr.* **2014**, *47*, 215−221.

(154) Henderson, R.; Baldwin, J. M.; Ceska, T. A.; Zemlin, F.; Beckmann, E.; Downing, K. H. Model for the structure of bacteriorhodopsin based on high-resolution electron cryo-microscopy. *J. Mol. Biol.* **1990**, *213*, 899−929.

(155) Kühlbrandt, W.; Wang, D. N.; Fujiyoshi, Y. Atomic model of plant light-harvesting complex by electron crystallography. *Nature* **1994**, *367*, 614−621.

(156) Grigorieff, N.; Ceska, T. A.; Downing, K. H.; Baldwin, J. M.; Henderson, R. Electron-crystallographic refinement of the structure of bacteriorhodopsin. *J. Mol. Biol.* **1996**, *259*, 393−421.

(157) Henderson, R.; Unwin, N. T. Three-dimensional model of purple membrane obtained by electron microscopy. *Nature* **1975**, *257*, 28−32.

(158) Glaeser, R. M.; Downing, K. H. High-resolution electron crystallography of protein molecules. *Ultramicroscopy* **1993**, *52*, 478−486.

(159) Subramanian, G.; Basu, S.; Liu, H.; Zuo, J. M.; Spence, J. C. H. Solving protein nanocrystals by cryo-EM diffraction: multiple scattering artifacts. *Ultramicroscopy* **2015**, *148*, 87−93.

(160) Clabbers, M. T. B.; Abrahams, J. P. Electron diffraction and three-dimensional crystallography for structural biology. *Crystallogr. Rev.* **2018**, *24*, 176−204.

(161) Henderson, R. The potential and limitations of neutrons, electrons and X-rays for atomic resolution microscopy and unstained biological molecules. *Q. Rev. Biophys.* **1995**, *28*, 171−193.

(162) Martin, D. C.; Chen, J.; Yang, J.; Drummy, L. F.; Kübel, C. High resolution electron microscopy of ordered polymers and organic molecular crystals: Recent developments and future possibilities. *J. Polym. Sci., Part B: Polym. Phys.* **2005**, *43*, 1749−1778.

(163) Kolb, U.; Gorelik, T. E.; Mugnaioli, E.; Stewart, A. Structural characterization of organics using manual and automated electron diffraction. *Polym. Rev.* **2010**, *50*, 385−409.

(164) Li, X.; Mooney, P.; Zheng, S.; Booth, C. R.; Braunfeld, M. B.; Gubbens, S.; Agard, D. A.; Cheng, Y. Electron counting and beam-induced motion correction enable near-atomic-resolution single-particle cryo-EM. *Nat. Methods* **2013**, *10*, 584−590.

(165) Llopart, X.; Campbell, M.; Dinapoli, R.; San Segundo, D.; Pernigotti, E. Medipix2: A 64-k pixel readout chip with 55 μm square elements working in single photon counting mode. *IEEE Trans. Nucl. Sci.* **2002**, *49*, 2279−2283.

(166) Jiang, L.; Georgieva, D.; Nederlof, I.; Liu, Z.; Abrahams, J. P. Image processing and lattice determination for three-dimensional nanocrystals. *Microsc. Microanal.* **2011**, *17*, 879−885.

(167) Smeets, S.; Wan, W. Serial electron crystallography: merging diffraction data through rank aggregation. *J. Appl. Crystallogr.* **2017**, *50*, 885−892.

(168) Arndt, U. W.; Wonacott, A. J. *The rotation method in crystallography*; Elsevier/North-Holland: Amsterdam, 1977.

(169) Trampari, S.; Valmas, A.; Logotheti, S.; Saslis, S.; Fili, S.; Spiliopoulou, M.; Beckers, D.; Degen, T.; Nenert, G.; Fitch, A. N.; Calamiotou, M.; Karavassili, F.; Margiolaki, I. J. *J. Appl. Crystallogr.* **2018**, *51*, 1671−1683.